

## New Formation Mechanisms of Pores and Cracks in Micro-arc Oxidation Coatings on 6061 Aluminum Alloy with High Temperature Oxide Prefab Film

Guo-rui WU<sup>1,2</sup>, Dong-dong WANG<sup>1</sup>, Xin-tong LIU<sup>1</sup>, Mingjia WANG<sup>1</sup>, Dong CHEN<sup>1</sup>, Yekang WU<sup>1</sup>, Dejiu Shen<sup>1\*</sup>

<sup>1</sup> State Key Laboratory of Metastable Materials Science and Technology, College of Materials Science and Engineering, Yanshan University, Qinhuangdao 066004, P.R. China

<sup>2</sup> CITIC Dicastal Limited by Share Ltd, Qinhuangdao 066000, P.R. China

**crossref** <http://dx.doi.org/10.5755/j02.ms.24210>

Received 16 September 2019; accepted 25 November 2019

Prior to micro-arc oxidation (MAO) treatment, a layer of high temperature oxide (HTO) prefab film was fabricated on the surface of 6061 aluminum alloy specimens. The formation mechanisms of the cracks and pores in the MAO coatings were investigated by means of Mg element as the tracer. The results showed that there were several different formation mechanisms for the pores and cracks formed in the MAO coatings as follows. Some of pores were attributed to the residual micro-discharge channels, and the others were attributed to the residual uncovered concave regions locating among the surrounding convex regions. The difference in oxide phase composition caused by the compositional fluctuations in the coating weakened the bond strength at the phase interface and resulted in forming cracks between every two convex regions. Some of cracks were resulted from the solidification and shrinkage of molten coating materials, and the others were resulted from the poor connection between every two convex regions. The surface morphology and the content of each element of the MAO coating were determined using scanning electron microscopy (SEM) equipped with energy dispersive X-ray spectroscopy (EDS).

*Keywords:* micro-arc oxidation coatings, cracks, pores, formation mechanisms, Mg tracer.

### 1. INTRODUCTION

Micro-arc oxidation (MAO), sometime termed as plasma electrolytic oxidation (PEO), is a promising surface modification technique, which allows a ceramic coatings to metallurgically integrate on the surface of valve metals and their alloys, such as Al, Mg and Ti [1–7]. MAO is considered as an effective technique to replace the conventional anodizing processes by which some surface properties (high hardness, good wear and corrosion resistance, biomedical and photo-catalytic usage) of the processed materials can be improved for applications [3, 6, 8]. However, the cracks and pores formed in the coatings during MAO processes are detrimental to the corrosion and wear resistances of the coatings [6, 7, 9, 10]. Therefore, it is important to investigate the formation mechanisms of the cracks and pores in the coatings.

MAO coating processes are actually quite complicated, which not only lead to the growth of MAO coatings, but also promote the formation of the pores and cracks [6, 7, 10–12]. The growth of MAO coatings is dependent on the continuous formation of the fresh oxide coating material accompanying with the moving micro-discharges caused by the dielectric breakdown of coatings. During MAO process, the concentrated anodic current provided the energy which could be partially used to instantaneously heat local oxide coating materials up to a high temperature of about 8000 K [13–15]. When micro-discharges were extinguished, some of molten oxide

coating materials were cooled down rapidly due to surrounding electrolyte before blocking off the discharge breakdown channels of the coatings, thus the residual pores appeared on the coating surface [15–18]. In addition, the formation of some cracks in MAO coatings, especially in the mid-to late-periods, is resulted from the release of the internal stresses coming from the sudden contraction and shrinkage of the oxide coatings due to the solidification of molten oxide coating materials and dehydration reaction of some MAO products, respectively [10, 15, 19]. In the previous works [10, 20], a high-temperature-oxidation (HTO) treatment was conducted before the MAO process of 6061 aluminum alloy, and the HTO prefab film was involved in the MAO coatings during the MAO process, which was identified by means of the Mg element distribution analysis from the substrate across the HTO-MAO coating.

### 2. EXPERIMENTAL DETAILS

6061Al alloy specimens with dimensions of 15 mm × 15 mm × 1 mm were machined as the substrates to be coated by MAO process. Before the HTO or MAO process, the specimens were burnished successively by 2000# and 3000# SiC abrasive paper, and ultrasonic cleaned in acetone, then washed with distilled water, and finally dried in air stream.

A magnesium-rich oxide film was prepared on the specimens during the HTO process before the MAO process, which has been described in the previous study [10]. In this work, a home-made pulsed bi-polar system was used as the MAO power supply and a constant current

\* Corresponding author. Tel.: +86 335 8055799.  
E-mail address: [DejiuShen@163.com](mailto:DejiuShen@163.com) (D. Shen)

density mode of  $4.4 \text{ A/dm}^2$  was applied on the sample during the MAO process. The electrolyte was prepared with 27 g/l  $\text{Na}_2\text{SiO}_3$ , 33 g/l  $(\text{NaPO}_3)_6$ , 4.3 g/l  $\text{Na}_2\text{SO}_4$  and 8 g/l  $\text{NaOH}$  in deionized water (pH 12.5). The MAO duration was set as 1, 2, 4, 8, 45 min, respectively. After the MAO process, the MAO-coated samples were washed thoroughly with deionized water and dried in air stream. The coating surface morphologies and the elemental distribution were analyzed by the scanning electron microscopy (SEM, Hitachi S-4800) and the energy-dispersive spectrometer (EDS) equipped on the SEM, respectively. The EDS tests were conducted at an accelerating voltage of 20 kV and a high probe current with a work distance of 15 mm.

### 3. RESULTS AND DISCUSSION

#### 3.1. Characterization of the HTO film

The typical surface and cross section SEM images and the main element distributions of the HTO film are shown in Fig. 1. Some relatively light gray and dark gray regions can be distinguished from each other on the film surface. It shows that the HTO film is, on some level, loose and discontinuous. The EDS spectra from the two types of regions labeled A and B, respectively, in Fig. 1 a are presented in Fig. 1 b. The results show that region A is much richer in Mg and O elements, suggesting that the content of magnesium oxide in the light gray regions is much higher than that in the dark gray ones, meanwhile, the film of the former regions is thicker compared with the

latter ones due to greater amounts of oxide products. The cross section of the HTO film and the EDS line analyses of Al, Mg and O marked in Fig. 1 c are shown in Fig. 1 c and d, which reveals that the HTO film has a much higher Mg/Al ratio compared to the substrate, implying that Mg atoms in the substrate were diffusing across the substrate towards the sample surface during the high temperature oxidation process, so as to supplement the more rapid consumption of magnesium atoms due to higher oxidation activity of element Mg than that of element Al. Thus, it can be seen that the substrate could change its surface state and prompt the Mg atoms migrating from the substrate inside to the surface.

#### 3.2. Formation processes of pores and cracks in the MAO coatings

Generally, the phase composition of MAO coatings consists of crystalline and amorphous phases due to the local conditions of high temperature sintering, melt quenching during MAO processes [10, 12, 13, 19]. The natural outcome of such a process is production of the heterogeneous microstructure with pores and cracks of the coatings [15].

Fig. 2 shows the surface morphologies of the MAO coatings produced on the 6061 aluminum alloy with the HTO prefab film for different time periods. The EDS analysis results corresponding to various typical micro-regions on the MAO coatings are shown in Fig. 3.

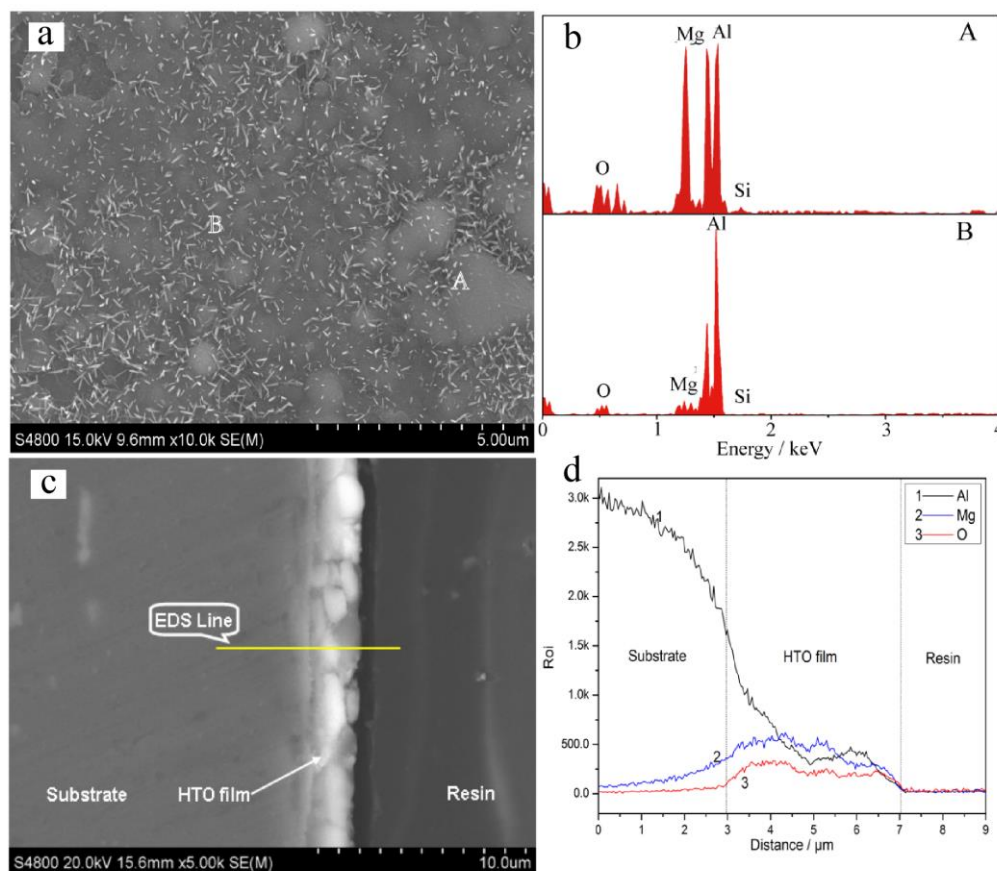


**Fig. 1.** a, c – surface and cross-sectional SEM images; b – point EDS spectra; d – line EDS spectra of the HTO film

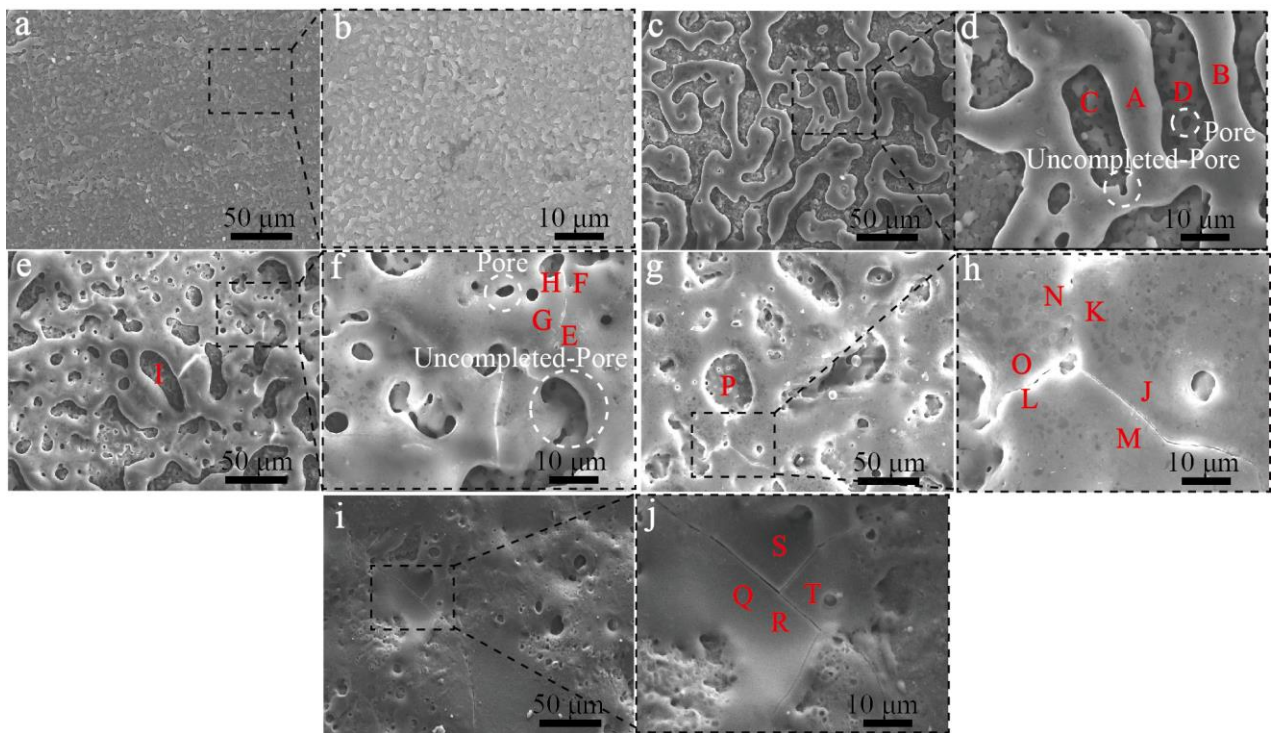


**Fig. 2.** Surface morphology of the MAO coatings: a, b–1 min; c, d–2 min; e, f–4 min; g, h–8 min; i, j–45 min; b, d, f, h, j magnifications of the boxes in a, c, e, g, i respectively

These pits seem to be inherited from the HTO prefab film (Fig. 1 and Fig. 2 b). What happened at 2 min was that some network areas with a lot of wormlike protrusions appeared on the flat surface, and many concave regions were formed among the convex worm-like regions (Fig. 2 c and d).

It is more interesting that the Mg contents at the convex and concave regions on the coatings are obviously different from each other based on the EDS examination (Fig. 3). Contents of Mg at regions A, B, C and D are 22.12 %, 20.14 %, 2.83 % and 3.28 %, respectively. It can be concluded that the Mg content at regions A and B representing the convex regions is much higher than that at regions C and D representing the concave regions, indicating that the regions with higher Mg content are more favorable to the formation of coating material compared to the regions with lower Mg content in the MAO process. In addition, the Mg contents at all the four spots above on the MAO coatings exceed that in the 6061 aluminum alloy substrate, being consistent with the EDS analysis result for the HTO prefab film shown in Fig. 1 d. As the MAO process continued, the area of the convex regions increased and the area of the concave regions decreased, so that more and more concave regions became round or elliptical pores, as shown in Fig. 2 e–h. The bubbles that come from the front of reactions during the process of MAO will be liberated and expelled through the discharge channel. Thus the formation of those round and elliptical pores may be the result of bubbles resisting the flow of the melting oxide films [4, 9]. Meanwhile, the Mg content at the concave regions (such as 0.31 % at spot I for 4 min and 0.48 % at spot P for 8 min) is still much lower than those at the convex regions (such as 9.03 % at spot E for 4 min and 11.01 % at spot M for 8 min), similar to the

results at 2 min (see Fig. 3). The surface morphology of MAO coating formed for 45 min is shown in Fig. 2 i and j, and it can be observed that the concave regions had already disappeared and the convex regions had already been connected together with each other, between the concave regions and the convex regions becoming indistinguishable. Now, the coating surface is relative flat and level compared with the coatings formed for 4 min and 8 min, and it can be also seen obviously that there were many pores originated in the evolution of discharge channels and the micro-cracks resulted from the solidification and shrinkage of melt oxide coating materials. As shown in Fig. 3, the Mg content in the convex regions decreased with prolonging the MAO process. With the prolonging of the MAO process, the Mg element in the MAO coating will be diluted by the alumina produced by plasma discharges. Further, in the middle- to late- stage of MAO process, the Mg-poor regions, in where plasma discharge is difficult to occur at the early stage, become the current weak regions of the existing coating (concave). Therefore, the plasma discharges will occur in these regions and form convex structures. The convex structures formed at this region (previous concave region) is similar to the convex structure formed at the Mg-rich region, but the Mg content of the coating is much less than that of the latter.

For the cracks in the coating produced for 4 min, as shown in Fig. 2 e and f, the Mg contents at the four points designated as E, F, G, H on both sides of the crack were shown in Fig. 3. It can be known that the Mg contents at spots E (9.03 %) and F (7.63 %) are much higher than those at spots G (1.82 %) and H (0.94 %), and the Mg contents at spots G, H are slightly higher than that in the original substrate. As discussed previously, the difference

in Mg contents at the different types of regions surrounding the cracks can be attributed to the different coating materials coming from different convex regions. It is suggested that the fresh molten oxide material was ejected from the discharge breakdown channels, then flowed around and connected to the previous solid oxide material, resulting in the formation of cracks, for such connections were poor. Based on the EDS results shown in Fig. 3, it can be known that the Mg contents in the three regions surrounding the cracks shown in Fig. 2 h are obviously different, i.e., those at spots L (9.88 %) and M (11.01 %) are higher than those at spots N (6.47 %) and O (5.93 %), and much higher than those at spots J (0.95 %),

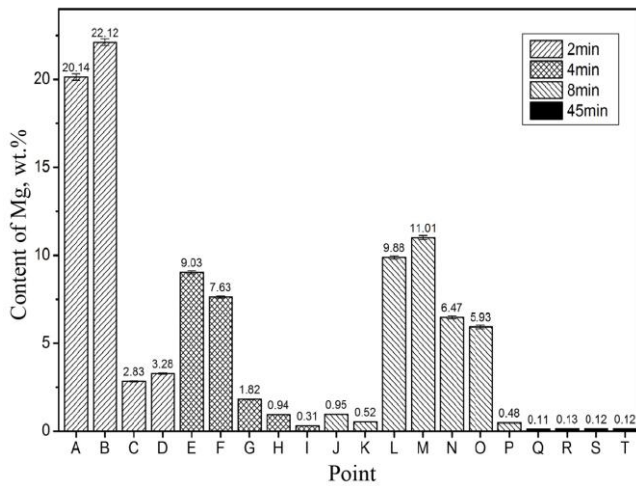


**Fig. 3.** Contents of element Mg at the typical micro-regions marked in Fig. 2

K (0.52 %), which indicates that the cracks shown in Fig. 2 h resulted from the convergence of three pieces of coating materials. This result proves that the cracks can be formed at such junctions once again. For the cracks in the coating developed for 45 min, as shown in Fig. 2 i and j, the Mg contents at the four points designated as Q, R, S, T were shown in Fig. 3. It can be known from Fig. 3 that the Mg contents at spots Q, R, S and T were similar to each other, indicating that the melt at the location of the crack was the eruption of the plasma discharge from the same position (concave regions), and its formation is due to the rapid solidification of molten oxide coating material. It is well known that the pores can be formed at the dead discharge sites, and the cracks on the MAO coating can be

formed by the stress release and thermal shock of the solid oxide. The above data, however, show that there are some new formation way for the pores and new formation process for the cracks on the MAO surface. As described by Fig. 4, some molten oxide produced by plasma discharges are generated at the Mg-rich region on the surface of the HTO film, and solid into convex oxide (pancake structures). With the increase of the number of the plasma discharge, such convex oxide proliferates and connected with each other. Meanwhile, these Al-rich regions, where is difficult to arouse plasma discharges compare to the Mg-rich region, are encircled by the convex oxide generated at the Mg-rich region, and some shallow pores are formed in the Al-rich region, as shown by Fig. 4 b. When the dielectricity of the Mg-rich region increases to a certain value due to the formation of the MAO coating, the concave pores play a role of weak sites in sample surface, and plasma discharges are ignited at these concave regions. Since the presence of Mg-rich (Al-poor) and Al-rich (Mg-poor) regions on the surface, as shown in Fig. 1, Fig. 2 and Fig. 3, there are some differences in the chemical composition between the convex oxide and the newly formed oxide at the concave pores, which causes a poor binding force at junction of the two typical oxides and induces cracks, as illustrated by Fig. 4.

#### 4. CONCLUSIONS

A high temperature oxide film was prefabricated on 6061 Al alloy, then the MAO treatment was conducted on the specimens with the high temperature oxide film, and the formation mechanisms of pores and cracks on the MAO coatings were investigated by means of element Mg as the tracer. The difference in oxide phase composition caused by the compositional fluctuations in the coating can weaken the bond strength at the phase interface, thereby weakening the bond strength at the phase interface and forming cracks. Besides some general formation mechanisms of pores on the MAO coatings, two a new formation mechanisms for some pores and cracks were proposed as follows. The formation of a part of pores was attributed to residual concave regions uncovered with the surrounding convex regions.

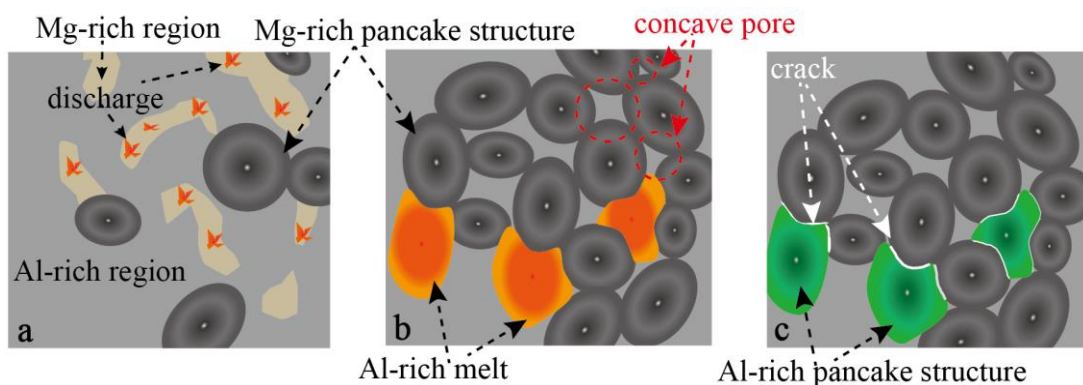


**Fig. 4.** Schematic of the formations of concave pores and some cracks

## Acknowledgments

This work was supported by National Natural Science Foundation of China (No.51171167) and Hebei Province Natural Science Foundation of China (Nos. A2015203348 and B2015203406).

## REFERENCES

1. **Vakili-Azghandi, M., Fattah-alhosseini, A., Keshavarz, M.K.** Effects of Al<sub>2</sub>O<sub>3</sub> Nano-Particles on Corrosion Performance of Plasma Electrolytic Oxidation Coatings Formed on 6061 Aluminum Alloy *Journal of Materials Engineering and Performance* 25 2016: pp. 5302–5313. <http://dx.doi.org/10.1007/s11665-016-2405-9>
2. **Fatimah, S., Yang, H.W., Kamil, M.P., Ko, Y.G.** Control of Surface Plasma Discharge Considering the Crystalline Size of Al Substrate *Applied Surface Science* 47 2018: pp. 60–67. <http://dx.doi.org/10.1016/j.apsusc.2017.12.208>
3. **Wu, Y.K., Yang, Z., Wang, R.Q., Wu, G.R., Chen, D., Wang, D.D., Liu, X.T., Li, D.L., Guo, C.H., Yu, S.X., Shen, D.J., Nash, P.** An Investigation of Microstructure Evolution for Plasma Electrolytic Oxidation (PEO) Coated Al in an Alkaline Silicate Electrolyte *Surface and Coatings Technology* 351 2018: pp. 136–152. <http://dx.doi.org/10.1016/j.surfcoat.2018.07.055>
4. **Wang, R.Q., Wu, Y.K., Wu, G.R., Chen, D., He, D.L., Li, D., Guo, C., Zhou, Y., Shen, D., Nash, P.** An Investigation about the Evolution of Microstructure and Composition Difference between Two Interfaces of Plasma Electrolytic Oxidation Coatings on Al *Journal of Alloys and Compounds* J753 2018: pp. 272–281. <http://dx.doi.org/10.1016/j.jallcom.2018.04.077>
5. **Ji, S., Weng, Y., Wu, Z., Ma, Z., Tian, X., Fu, R.K.Y., Hai, L., Wu, G., Chu, P.K., Feng, P.** Excellent Corrosion Resistance of P and Fe Modified Micro-Arc Oxidation Coating on Al Alloy *Journal of Alloys and Compounds* 710 2017: pp. 452–459. <http://dx.doi.org/10.1016/j.jallcom.2017.03.303>
6. **Chen, D., Wang, R., Huang, Z., Wu, Y., Zhang, Y., Wu, G., Li, D., Guo, C., Jiang, G., Yu, S., Shen, D., Nash, P.** Evolution Processes of the Corrosion Behavior and Structural Characteristics of Plasma Electrolytic Oxidation Coatings on AZ31 Magnesium Alloy *Applied Surface Science* 434 2018: pp. 326–335. <http://dx.doi.org/10.1016/j.apsusc.2017.09.232>
7. **Wang, D.D., Liu, X.T., Su, Y., Wu, Y.K., Yang, Z., Han, H.P., Zhang, X.Z., Wu, G.R., Shen, D.J.** Influences of Edge Effect on Microstructure and Corrosion Behaviour of PEO Coating *Surface Engineering* 2019: pp. 184–191. <http://dx.doi.org/10.1080/02670844.2019.1644935>
8. **Gnedenkov, S.V., Khrisanfova, O.A., Zavidnaya, A.G., Sinebryukhov, S.L., Egorkin, V.S., Nistratova, M.V., Yerokhin, A., Matthews, A.** PEO Coatings Obtained on an Mg–Mn Type Alloy Under Unipolar and Bipolar Modes in Silicate-Containing Electrolytes *Surface & Coatings Technology* 204 2010: pp. 2316–2322. <http://dx.doi.org/10.1016/j.surfcoat.2009.12.024>
9. **Ko, Y.G., Lee, K.M., Lee, B.U., Shin, D.H.** An Electrochemical Analysis of AZ91 Mg Alloy Processed by Plasma Electrolytic Oxidation Followed by Static Annealing *Journal of Alloys and Compounds* 509 2011: pp. S468–S472. <http://dx.doi.org/10.1016/j.jallcom.2010.12.040>
10. **Shen, D., Zou, J., Wu, L., Liu, F., Li, G., Cai, J., He, D., Ma, H., Jiang, G.** Effect of High Temperature Oxidation Prefab Film on Formation of Micro-Arc Oxidation Coatings on 6061aluminum Alloy *Applied Surface Science* 265 2013: pp. 431–437. <http://dx.doi.org/10.1016/j.apsusc.2012.11.024>
11. **Liu, C., He, D., Yan, Q., Huang, Z., Liu, P., Li, D., Jiang, G., Ma, H., Nash, P., Shen, D.** An Investigation of the Coating/Substrate Interface of Plasma Electrolytic Oxidation Coated Aluminium *Surface and Coatings Technology* 280 2015: pp. 86–91. <http://dx.doi.org/10.1016/j.surfcoat.2015.08.050>
12. **Shen, D., He, D., Liu, F., Guo, C., Cai, J., Li, G., Ma, H.** Effects of Ultrasound on the Evolution of Plasma Electrolytic Oxidation Process on 6061Al Alloy *Ultrasonics* 54 2014 1065–1070. <http://dx.doi.org/10.1016/j.ultras.2013.12.011>
13. **Wang, D.D., Liu, X.T., Wu, Y.K., Han, H.P., Yang, Z., Su, Y., Zhang, X.Z., Wu, G.R., Shen, D.J.** Evolution Process of The Plasma Electrolytic Oxidation (PEO) Coating Formed on Aluminum in an Alkaline Sodium Hexametaphosphate ((NaPO<sub>3</sub>)<sub>6</sub>) Electrolyte *Journal of Alloys and Compounds* 798 2019: pp. 129–143. <http://dx.doi.org/10.1016/j.jallcom.2019.05.253>
14. **Hussein, R.O., Nie, X., Northwood, D.O., Yerokhin, A., Matthews, A.** Spectroscopic Study of Electrolytic Plasma and Discharging Behaviour During the Plasma Electrolytic Oxidation (PEO) Process *Journal of Physics D: Applied Physics* 43 2010: pp. 105203–105215. <http://dx.doi.org/10.1088/0022-3727/43/10/105203>
15. **Hussein, R.O., Nie, X., Northwood, D.O.** An Investigation of Ceramic Coating Growth Mechanisms in Plasma Electrolytic Oxidation (PEO) Processing *Electrochimica Acta* 112 2013: pp. 111–119. <http://dx.doi.org/10.1016/j.electacta.2013.08.137>
16. **Troughton, S.C., Nominé, A., Nominé, A.V., Henrion, G., Clyne, T.W.** Synchronised Electrical Monitoring and High Speed Video of Bubble Growth Associated with Individual Discharges During Plasma Electrolytic Oxidation *Applied Surface Science* 359 2015: pp. 405–411. <http://dx.doi.org/10.1016/j.apsusc.2015.10.124>
17. **Yerokhin, A.L., Snizhko, L.O., Gurevina, N.L., Leyland, A., Pilkington, A., Matthews, A.** Discharge Characterization in Plasma Electrolytic Oxidation of Aluminium *Journal of Physics D: Applied Physics* 36 2003: pp. 2110. <http://dx.doi.org/10.1088/0022-3727/36/17/314>
18. **Zhu, L., Guo, Z., Zhang, Y., Li, Z., Sui, M.** A Mechanism for The Growth of a Plasma Electrolytic Oxide Coating on Al *Electrochimica Acta* 208 2016: pp. 296–303. <http://dx.doi.org/10.1088/0022-3727/36/17/314>
19. **Hussein, R.O., Northwood, D.O., Nie, X.** The influence of Pulse Timing and Current Mode on the Microstructure and Corrosion Behaviour of a Plasma Electrolytic Oxidation (PEO) Coated AM60B Magnesium Alloy *Journal of Alloys and Compounds* 541 2012: pp. 41–48. <http://dx.doi.org/10.1016/j.jallcom.2012.07.003>
20. **Shen, D., Li, G., Guo, C., Jie, Z., Cai, J., He, D., Ma, H., Liu, F.** Microstructure and Corrosion Behavior of Micro-Arc Oxidation Coating on 6061 Aluminum Alloy Pre-Treated by High-Temperature Oxidation *Applied Surface Science* 287 2013: pp. 451–456. <http://dx.doi.org/10.1016/j.apsusc.2013.09.178>



© Wu et al. 2021 Open Access This article is distributed under the terms of the Creative Commons Attribution 4.0 International License (<http://creativecommons.org/licenses/by/4.0/>), which permits unrestricted use, distribution, and reproduction in any medium, provided you give appropriate credit to the original author(s) and the source, provide a link to the Creative Commons license, and indicate if changes were made.